AT622 Section 6
The Earth

This section provides students with an understanding of the radiative budget of the Earth and seeks to put this budget in the context of the total energy budget of the planet thus placing the topic of atmospheric radiation in a broader context.

KEY REFERENCES

Barkstrom, B., 1984: The earth radiation budget experiment (ERBE), *Bull. Amer. Met. Soc.*, **11**, 1170-1185.

Kiehl, J. T. and K. E. Trenberth, 1997: Earth's annual global mean energy budget, *Bull. Amer. Met. Soc.*, **78**, 197-208.

Ramanathan, 1987: Role of earth radiation budget studies on climate and general circulation research, *JGR*, **92**, 4075 - 4095.

Ramanathan, Barkstrom and Harrison, 1989: Climate and the earth's radiation budget, *Physics Today*, 22-37.

Stephens, Campbell and Vonder Haar, 1981: Earth radiation budgets, *JGR*, **86**, 9739 - 9760.

6.1 The Earth's Radiation Budget

A fundamental property of the Earth's climate system is the radiative budget defined as

$$F_{net} = \frac{Q_\odot}{4}(1-\alpha) - F_\infty \tag{6.1}$$

referred to as the Earth's Radiation Budget (ERB). In this definition, F_{net} is the net radiation imbalance at the top of the atmosphere, $Q_\odot$ is the solar constant (remember where the factor of 4 comes from?), α is the albedo of the planet and F_∞ is the outgoing emitted longwave radiation. We believe that on the annual and global mean the planet as a whole is in radiative equilibrium (an assertion supported by satellite measurements—at least to the accuracy of the measurements), thus $F_{net} = 0$ and

$$\frac{Q_\odot}{4}(1-\overline{\alpha}) = \overline{F}_\infty \tag{6.2}$$

where the overbar emphasizes the global-annual average of the specified quantities.

(a) The Planetary Temperature

It is sometimes convenient to consider F_∞ in terms of an equivalent blackbody emission (of course it is not purely blackbody as we have already seen). If we write $\overline{F}_\infty = \sigma T_p^4$, then this balance can be written as

$$\underbrace{\frac{Q_\odot}{4}(1-\alpha)}_{\text{absorbed solar energy}} = \underbrace{\sigma T_p^4}_{\text{emitted energy}} \tag{6.3}$$

It follows from this balance that

$$T_p = \left(\frac{Q_\odot (1-\alpha)}{4\sigma} \right)^{1/4} \tag{6.4}$$

where $Q_\odot$ depends on the sun-earth distance. Figure 6.1 graphically presents Eqn. (6.4) and Table 6.1 provides values of various quantities that help define the radiative equilibrium for various planets. Note for example that T_p for Venus is similar to that of Earth even though $Q_\odot$ is almost twice as large.

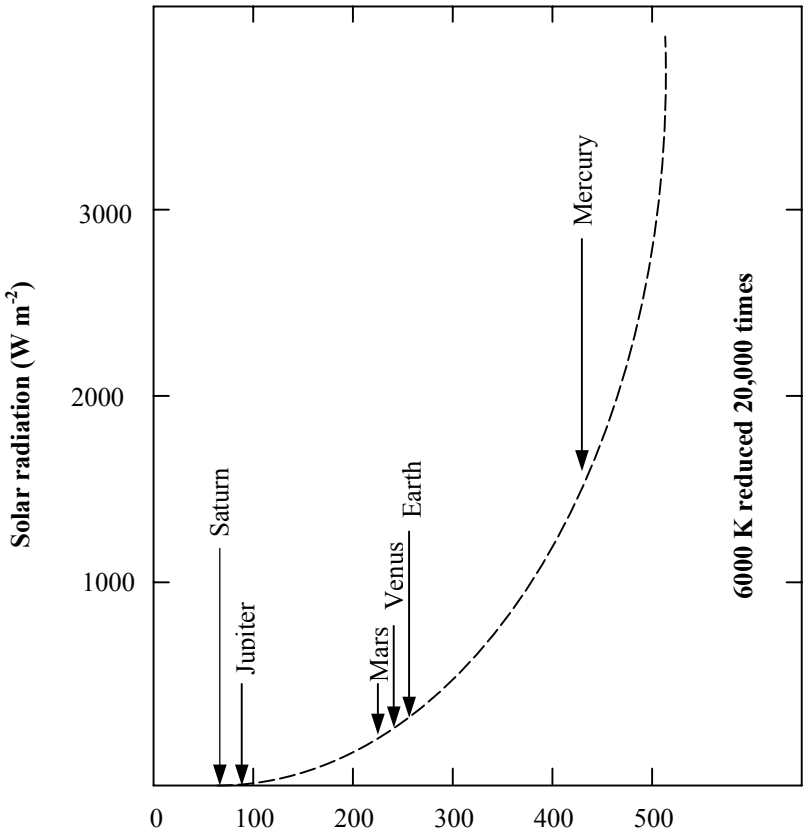

Fig. 6.1 The Stephan-Boltzmann law equates the emitted heat radiation to 5.67 × 10^{-5} × (temperature)^4. Effective temperatures of the sun and planets are shown in Table 6.1.

The value of T_p for Earth is 253 K, which is much too cold to be representative of the globally averaged surface temperature of 288 K (actually, T_p = 253 K is approximately the mean temperature of the 500 mb surface). The reason for the difference between the surface and planetary temperatures is that the Earth's atmosphere itself emits radiation. For temperatures typical of Earth, this emission occurs mainly in the infrared region of the electromagnetic spectrum with a peak wavelength around 10 μm (Section 3). The difference between T_p and the observed surface temperature, T_s, is therefore a measure of strength of the greenhouse effect.

Table 6.1 Effective temperatures of the sun and planets.

Planet	Distance from sun (10^4 km)	Flux of solar radiation (10^4 erg cm^{-3} sec^{-1})	Albedo	T_p
Mercury	58	9.2	0.058	442
Venus	108	2.6	0.71	244
Earth	150	1.4	0.33	253
Mars	228	0.60	0.17	216
Jupiter	778	0.049	0.73	87
Saturn	1430	0.015	0.76	63
Uranus	2870	0.0037	0.93	33
Neptune	4500	0.0015	0.84	32
Pluto	5900	0.00089	0.14	43

(b) The Evolutionary Theory of Planetary Atmospheres

In essence, the Earth's atmosphere is fairly transparent to solar radiation but opaque (except for the window region) to infrared radiation. Thus the surface is warmed by sunlight and maintained by radiation from the atmosphere. This produces an increase in surface temperature over the planetary temperature and is a phenomenon understood to be the greenhouse effect. This effect is obviously very different from planet to planet as a comparison between T_p and T_s, for the planets listed in Table 6.1. Of some interest to our overall understanding of the present state of the Earth's climate is how the Earth's atmosphere evolved with water vapor and CO_2 being released into the atmosphere. This sort of understanding is also important to the assessment of how our present climate might change with changing concentrations of these gases.

One hypothesis for the evolution of the climates of the three inner planets of the solar system is graphically portrayed in Fig. 6.2. The proposed evolution of the surface temperature of Venus, Earth, and Mars is shown as a function of the amount of water vapor in the atmosphere. This figure suggests that as water accumulates in the atmosphere, owing to the greenhouse effect, the surface temperature rises. It is thought that as more water vapor is added in the atmosphere of Venus, the temperature increases creating a runaway feedback (the so called **runaway greenhouse effect**). The atmosphere of Venus presently contains little water vapor. This is explained under the runaway hypothesis by requiring most of the water vapor to have reached the upper atmosphere where it photodissociated and ultimately escaped. The present strength of the greenhouse on Venus is maintained by the clouds and large abundance of CO_2. Both Earth and Mars are said to experience a **truncated greenhouse effect** such that increases in vapor are met with water phase changes.

In summary:

- MERCURY: all outgassed gases are stripped. No atmosphere.
- VENUS: sufficiently massive that important gases do not escape. Close enough to the sun that water phase transitions are not reached and an unbuffered runaway system is set up.
- EARTH: Particular T_p allows encounter of the H_2O phase transitions near the triple point. Thus Earth's climate is buffered by these phase changes, i.e., continued outgassing condenses into oceans and clouds or sublimes; partial pressure of gas cannot increase and feedback on the greenhouse effect is much weaker than it is (hypothesized) for Venus.
- MARS: Low T_p forces encounter with ice/vapor transition. Mars' climate is buffered as any H_2O outgassing sublimes to ice preventing further increases of gas partial pressure.

The present state of the atmospheres of Venus and Earth, in this view, is therefore largely a result of the proximity of the planet to the sun.

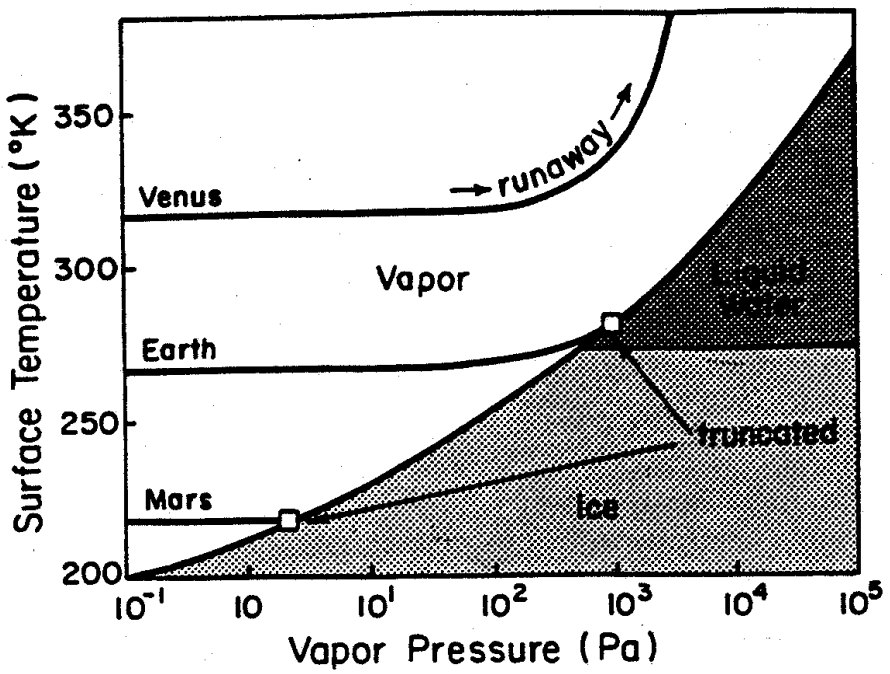

Fig. 6.2 The runaway greenhouse effect. The solid lines show how surface temperatures increase, due to the greenhouse effect, as water vapor accumulates in the atmospheres of the inner planets. On Mars and on Earth the increase is halted when the water vapor pressure is equal to the saturated vapor pressure (shown as the dark curve) and freezing or condensation occurs. Temperatures are higher on Venus because Venus is closer to the sun and saturation is never achieved. The temperature runs away. Note that the temperatures on the left-hand axis are not the same for Earth and Venus as the effective temperatures in Table 6.1. They differ because a different albedo has been used. (After S. I. Rasool and C. DeBergh, 1970) Source: (G. & W.).

6.2 Gray Body Transfer: The Role of Radiation on the Temperature Structure of the Atmosphere

It is instructive to study the role of infrared radiation in a simple climate model, in which the rather drastic assumption is made that the optical depth is independent of frequency. This is known as the "gray" approximation. To this end, we will consider the concept of gray body radiative transfer and further introduce the notion of radiative equilibrium—a notion that we will return to later.

In dealing with gray body transfer, let us begin with a monochromatic RTE

$$\mu \frac{dI(\tau,\mu)}{d\tau} = I(\tau,\mu) - B(T) \tag{6.5a}$$

$$-\mu \frac{dI(\tau,-\mu)}{d\tau} = I(\tau,-\mu) - B(T) \tag{6.5b}$$

Example 6.1: An estimate of the gray-body optical depth

The spectral optical depth is a complex function of wavelength and several ways of spectrally averaging τ exist. The approach used here is one appropriate to the radiative equilibrium arguments introduced to arrive at Eqn. (6.11) and follows from the following flux-mean mass absorption coefficient (Mihalas, 1978)

$$k_f = F_\infty^{-1} \int k_f F_{\infty,\lambda} d\lambda .$$

The contribution to τ by water vapor, carbon dioxide and other minor greenhouse gases present in the Earth's atmosphere obtained using k_f in Eqn. (6.6), is shown below. The spectral absorption data used to derive k_f are those tabulated by Rothman (1981). The total gray body optical depth derived from these data is $\tau = 3.9$ corresponding to $w = 28$ kg m^{-2}, which is close to the global mean values of w. The value $\tau = 3.9$ is larger than the value of the optical depth derived from later considerations. This highlights the ambiguity of the quantitative meaning of τ and to understand the value it is necessary to understand how it is derived. The advantage of the flux-weighted value is that it allows us to estimate τ from spectral integration and thus the contributions by individual gases. These contributions clearly emphasize the dominance of water vapor to the total gray body optical depth for the global mean conditions considered.

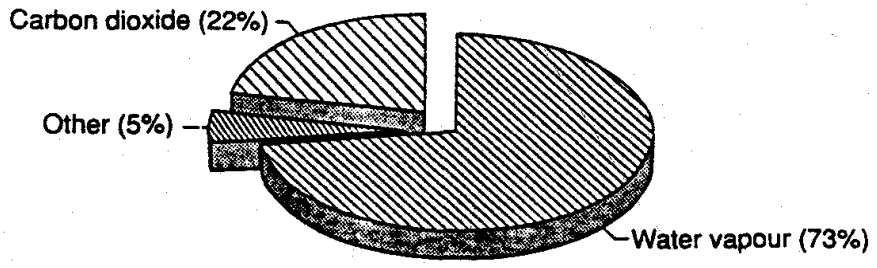

A pie diagram showing the percentage of the gray body optical depth due to water vapor and other greenhouse gases in the Earth's atmosphere based on typical mean global concentrations of these gases.

where I is the intensity, $\mu = \cos\theta$ where θ is the angle of the beam from the zenith. The optical depth is defined as

$$\tau = \int_z^\infty k \rho_a dz \qquad (6.6)$$

where k *is* the mass absorption coefficient, ρ_a is the density of the absorbing gas, and z is the lowest end point of the path. It is simple to cast these equations into equations for (see box below) upward (F^+) and downward (F^-) hemispheric fluxes,

$$\frac{dF^+}{d\tilde{\tau}} = F^+ - \pi B, \tag{6.7a}$$

$$-\frac{dF^-}{d\tilde{\tau}} = F^- - \pi B, \tag{6.7b}$$

where

$$\tilde{\tau} = \frac{3}{2}\tau .$$

We now introduce the gray body assumption, which means if we take $\tilde{\tau}$ to be independent of wavelength (we know that it is not), then we can treat the fluxes in Eqns. (6.7a and b) as broadband quantities and replace πB with σT^4. The factor of 3/2 is a form of *diffusivity factor* and its interpretation follows from the considerations discussed below.

Let us introduce the notion of radiative equilibrium, which for our purpose means that at the top of the atmosphere

$$F^+(\tilde{\tau} = 0) = \frac{Q_\odot}{4}(1-\alpha) = F_\infty \tag{6.8a}$$

where $Q_\odot$ is the global-annual mean incoming solar radiation at the top of the atmosphere and α is the planetary albedo **(note:** these are all broadband quantities). Radiative equilibrium also implies that throughout the atmosphere (why??)

$$F_{net} = F^+(\tilde{\tau}) - F^-(\tilde{\tau}) = const \tag{6.8b}$$

(we are also assuming that no solar radiation is absorbed in the atmosphere). Given this condition, it follows from Eqn. (6.7a) that

$$F^+(\tilde{\tau}) + F^-(\tilde{\tau}) = 2\pi B(\tilde{\tau})$$

and further from (6.8b) that

$$F^+(\tilde{\tau}) + F^-(\tilde{\tau}) = F_{net}\tilde{\tau} + C .$$

On combining these equations we obtain

$$B(\tilde{\tau}) = \frac{F_{net}}{2\pi}(\tilde{\tau} + 1) .$$

Example 6.2: A further derivation of the flux equations

It is a relatively simple matter to convert Eqns. (6.5a and b) into flux equations if we define a direction $\bar{\mu}$ such that the flux

$$F^+ = 2\pi\int_0^{+1} I(\mu)\mu d\mu = \pi I(\bar{\mu}).$$

Thus it is straightforward to write down the RTE at $\mu = \bar{\mu}$. By multiplying each side of this equation by a factor of π we arrive at Eqns. (6.7a and b) with $\bar{\mu}$ = 2/3.

The solution to these equations follows by first differencing these equations to yield

$$\frac{dF_{net}}{d\tilde{\tau}} = (F^+ + F^-) - 2\pi B \qquad (6.9a)$$

(remember F_{net} = (F^+ - F^-)) and summing the equations to obtain

$$\frac{d(F^+ + F^-)}{d\tilde{\tau}} = F_{net} \qquad (6.9b)$$

which provides two equations for the two unknowns F_{net} and (F^+ + F^-). We will now explore these solutions given an additional assumption about radiative equilibrium.

At the top of the atmosphere, we have $\tilde{\tau}$ = 0 and F^- = 0, so that $F_{net} = F_\infty$ and $C = F_{net}$. Further, under the gray body assumption

$$\sigma T^4(\tilde{\tau}) = \frac{F_\infty}{2}(\tilde{\tau} + 1) \qquad (6.10a)$$

At the bottom of the atmosphere, where $\tilde{\tau} = \tilde{\tau}_s$, we have $F^+ = \sigma T_s^4$ and it follows that

$$\sigma T_s^4 - F^-(\tilde{\tau}_s) = F_\infty$$

$$\sigma T_s^4 + F^-(\tilde{\tau}_s) = F_\infty(\tilde{\tau}_s + 1)$$

and that

$$\sigma T_s^4 = \frac{F_\infty}{2}[2 + \tilde{\tau}_s] \qquad (6.10b)$$

$$F_g^- = F^-(\tilde{\tau}_s) = \frac{F_\infty}{2}\tilde{\tau}_s \tag{6.10c}$$

at the surface.

Example 6.3: Skin temperatures and temperature discontinuities

The solutions represented by Eqns. (6.10a) and (6.10b) provide rather interesting insights into the temperature profiles that are predicted by these equations. One of the results of this model is an estimate of the 'skin' temperature, which we think of as a measure of the stratospheric temperature. We obtain this using Eqn. (6.10a) with $\tilde{\tau} = 0$

$$\sigma T^4(\tilde{\tau} = 0) = \frac{F_\infty}{2}$$

and with $F_\infty \approx 235$ Wm^{-2}, it follows that this temperature is T_{skin} = [117.5/5.68 $\times 10^{-8}$]$^{0.25}$ = 213 K.

The solutions in Eqns. (6.10a) and (6.10b) predict a discontinuity between the surface temperature T_s and the air temperature just above the ground $T(\tilde{\tau}_s)$. Differencing these equations and with $\tilde{\tau} = \tilde{\tau}_s$,

$$\sigma T_s^4 - \sigma T^4(\tilde{\tau}_s) = \frac{F_\infty}{2}.$$

The results of the model are presented in Fig. 6.3a, showing the profiles of upward and downward fluxes and the profile of the temperature that is contained in the profile of flux πB. Highlighted are the skin temperatures and the discontinuity at the surface. At first sight, the model does not seem to bear any resemblance to the real temperature profile. This is because the coordinate τ is not an easy coordinate to interpret. Let us suppose that τ is largely defined by water vapor and that

$$\rho(\mathrm{H_2O}) = \rho_0 e^{-z/H_{\omega v}}$$

where $H_{\omega v} \approx 2$ km. To simplify matters, we assume that τ varies with z in the same way $\rho(\mathrm{H_20})$ varies with z

$$\tau = \tau_s e^{-z/2} \tag{6.11}$$

and

$$\sigma T^4(z) = \frac{F_\infty}{2}\left[1 + \frac{3}{2}\tau * e^{-z/2}\right]$$

The profile of temperature with height equivalent to Fig. 6.3a is presented in Fig. 6.3b. For comparison, the profile defined by a 6 K km^{-1} lapse rate is presented. We note that the radiative equilibrium profile is

unstable throughout most of the atmosphere, at least to where the 6 K km^{-1} profile cuts the radiative equilibrium profile. This radiative equilibrium profile is unstable w.r.t. vertical motion and is destroyed by convection, which we may think of in this simple model as producing the constant lapse rate profile. Where the latter intersects the radiative equilibrium profile at about 10 km is where this simple model predicts the position of the tropopause.

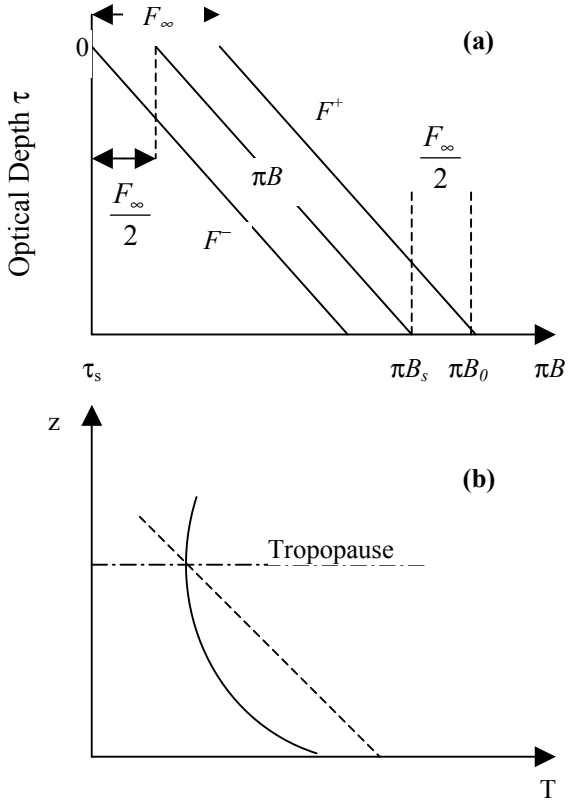

Fig. 6.3 (a) The flux profiles and blackbody function predicted by the simple gray body model as a function of optical depth. (b) The radiative equilibrium temperature profile as a function of altitude predicted by the flux model and assuming the profile of optical depth in Eqn. (6.11).

6.3 The Greenhouse Effect and Water Vapor Feedback

Theories of the evolution of the atmosphere of Venus are a subject of some debate. Conjectures other than the runaway greenhouse-hydrodynamic loss hypothesis have been forwarded to explain the present climate of Venus. A contrary view is that the atmosphere of Venus never contained water vapor at the levels required for the runaway hypothesis and that most of the planet's water remains fixed in its interior (Kaula 1990). Whether this runaway greenhouse model proposed for Venus actually occurred or not is not the issue here. The runaway hypothesis serves to illustrate a feedback between water vapor, the greenhouse effect, and the surface temperature of the planet—a feedback that is also thought to occur on Earth although on a much more limited scale (Manabe and Wetherald 1967). In fact, it is the water vapor feedback in present day climate models that contributes the major portion of the global warming predicted for increasing concentrations of atmospheric CO_2.

Figure 6.4a provides a schematic depiction of how this water vapor feedback is thought to take place under the influence of increasing concentrations of carbon dioxide. As the sea surface temperature warms

from the rising levels of CO_2, increased evaporation of water from the oceans leads to an enhanced water vapor content of the atmosphere (Fig. 6.4a), which further warms the oceans. The total warming calculated by a typical climate model is also given in Fig 6.4a as is the amount of warming calculated for a doubling of CO_2 without any water vapor feedback. While these results apply to a specific climate model (Manabe and Wetherald 1967), most models give similar responses and half of the projected observations, like those shown in Fig. 6.4b, suggest that a kind of thermodynamic equilibrium exists between the sea surface temperature and water vapor content in a manner closely resembling the Clausius-Clapeyron relation.[1]

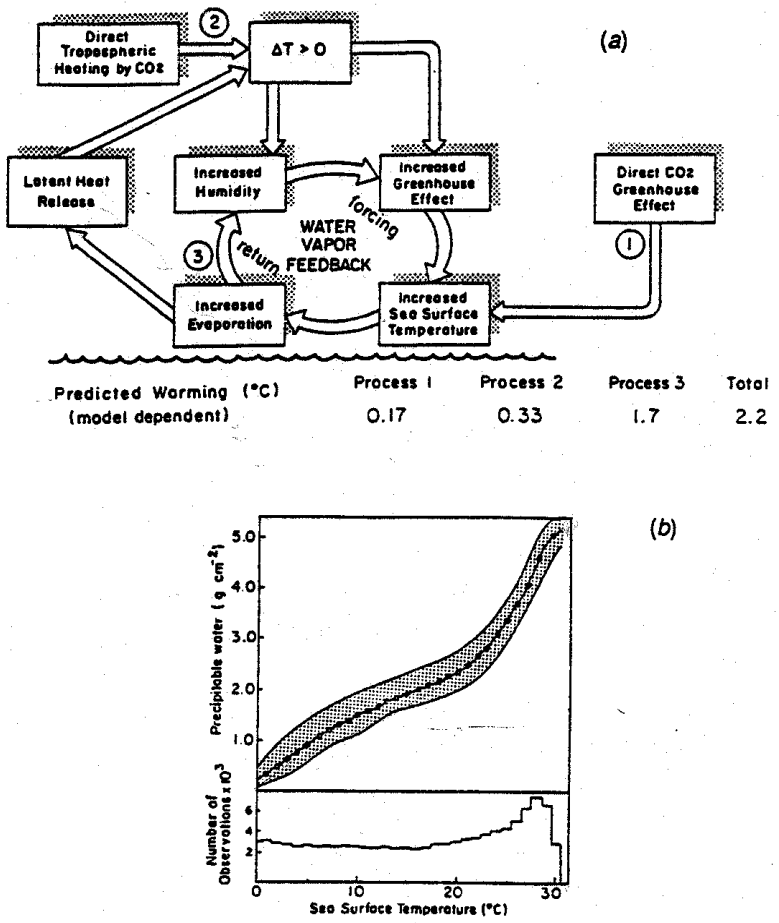

Fig. 6.4 *(a) An illustration of the water vapor feedback as it is thought to occur on Earth when triggered by a small warming induced by increasing atmospheric CO_2. The water vapor feedback is thought to account for more than half of the final warming simulated by present day climate models (adapted from Ramananthan, Manabe and Wetherald, 1967). (b) A necessary condition for the existence of water vapor feedback on Earth. Water vapor exists in equilibrium with the oceans in a way that is related to the sea surface temperature largely through the Clausius-Clapeyron relationship. The curve shown is established from thousands of observations of water vapor over the world's oceans (Stephens, 1990).*

[1] Other views have been expressed that the positive feedback does not operate to the extent predicted in current climate models. For further discussion see S. H. Schneider, 1990: The global warming debate heats up: an analysis and perspective, *Bull. Amer. Meteor. Soc.*, **71**, 1292-1304.

Unlike Venus, however, the water vapor feedback loop on Earth is interfered with by condensation of vapor into clouds, which in turn imparts a substantial influence of their own on the greenhouse effect. The actual way this interference by clouds takes place and the specific connection between water vapor, cloudiness, and the greenhouse effect on Earth are still not well understood, poorly observed, and largely unexplored.

(a) A simple Estimate of the Water Vapor Feedback

We can devise a simple way of estimating the strength of this feedback. Consider our energy budget and suppose we can seek to determine the magnitude of the perturbation of temperature ΔT_s due to a small change $\Delta Q_\odot$ in solar flux. It follows then that:

$$4\sigma T_p^3 \Delta T_p = \frac{\Delta Q_\odot}{4}(1-\alpha) = \Delta F_\infty \tag{6.12}$$

and then

$$\Delta T = \Delta F_\infty \left(\frac{T_{eq}}{4F_\infty} \right) = 0.63 \text{ K} \tag{6.13}$$

But this sensitivity does not take water vapor and its feedback into account. One way to think of the feedback is to consider Fig. 6.5 and

$$F_\infty = A + BT_s \tag{6.14}$$

where $A \approx 203.3$ W m^{-2} and B ≈ 2.09 W m^{-2} ° C^{-1}. It follows then that**:**

$$\Delta T = \frac{\Delta F}{B} = \frac{0.01(A+BT)}{B} \approx 1.12°\text{C} \tag{6.15}$$

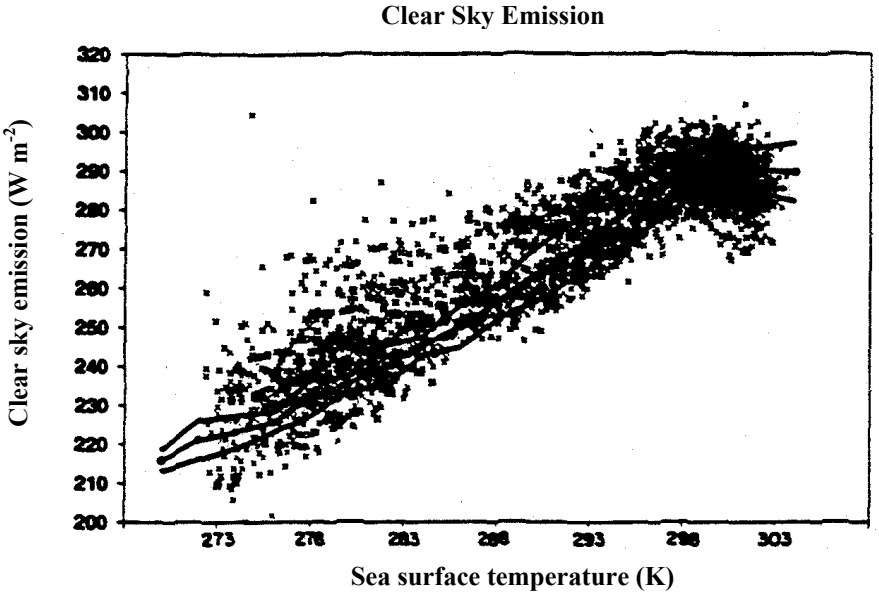

Fig. 6.5 The longwave flux emitted to space at different locations on Earth as a function of the surface temperature measured at that location (Stephens et al., 1993).

Thus the presence of an atmosphere (chiefly water vapor), which is modeled via the Budyko relationship (IR emission varies with T_s by a factor less than a T^4), increases the sensitivity of 'climate' to solar forcing by approximately a factor of two.

(b) Studying the Greenhouse Effect and Water Vapor Feedback from Space

It is not possible, in principle, to observe the direct effects of feedbacks occurring in the climate system since we observe the collections of responses. We can, however, observe key components of these feedbacks. First, let us introduce a measure of the greenhouse effect. Perhaps the simplest way is to use the difference between the mean radiating temperature of the planet and the surface temperature (Kondratyev and Moskalenko, 1984; Stephens and Tjemkes, 1992). However, the relationship between this temperature difference and the concentration of emitting species cannot be simply and conveniently defined. We will make use of our relationship in Eqn. (6.10b) and define a greenhouse parameter as

$$G = \frac{\sigma T_s^4}{F_\infty} = 0.5(\tilde{\tau}_s + 2) \tag{6.16}$$

or more generally

$$G = \frac{\sigma T_s^4}{F_\infty} = a + b\tau_s \tag{6.17}$$

where from Eqns. (6.8) and (6.10a), a = 1 and b = 3/4. This definition identifies the gray body optical depth as the key parameter in defining the strength of the greenhouse.

Let us simply assume that in the case of water vapor, the gray body optical depth is

$$\tau_s = \int k_f \rho_a dz \approx k_f w. \tag{6.18}$$

This assumption, together with Eqn. (6.17) then leads to the following (e.g., Stephens and Greenwald, 1991b)

$$G = a + cw\ . \tag{6.19}$$

The advantage of this relationship is that all factors in Eqn. (6.19) are independently observed over the global oceans, primarily from satellites. For example, the SST can be obtained from independent analyses of blended ship, buoy, and satellite data (e.g., Reynolds, 1984). The OLR available from ERBE data and w follow from microwave measurements. The annual, January and July monthly mean values of G derived in this way are plotted against corresponding mean values of w in Fig. 6.6. The solid line through the scatter of annual mean points depicts the average of these points and the slope parameter c = 0.00634 (kg m^{-2})$^{-1}$, which is estimated via a least squares fit of the data (shown as the solid line in Fig 6.6), is a measure of how the greenhouse effect changes for given changes in w and is potentially important in the analyses of water vapor feedback.

The relationship in Eqn. (6.19) may be explored using data over the Earth's oceans where suitable global measures of the SST, F_∞ and w are available from existing satellite observations. Since the relationship between w and SST is well defined, it is also possible to consider G as a function of SST. An example of this kind of relationship derived from satellite data is taken from Webb et al. (1994) and shown in Fig. 6.6a for July 1988 and Fig. 6.6b for January 1989. When plotted in this way with the

relationships for each hemisphere indicated by the different symbols, a dramatic seasonal branching of the relation between *G* and SST emerges. Webb et al. (1993) identify this as largely due to a seasonal effect associated with changes in the vertical profile of atmospheric temperature in the middle latitudes.

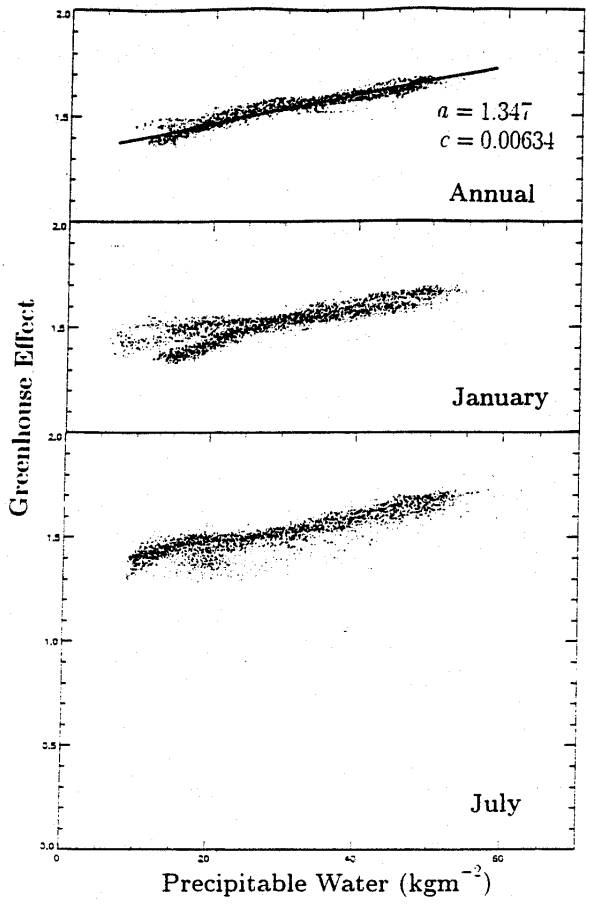

Fig. 6.6 The correlation of G with w based on annual mean (upper panel), 1989 January mean (middle panel), and 1988 July mean data (lower panel). The unit of c is (kgm^{-2})$^{-1}$.

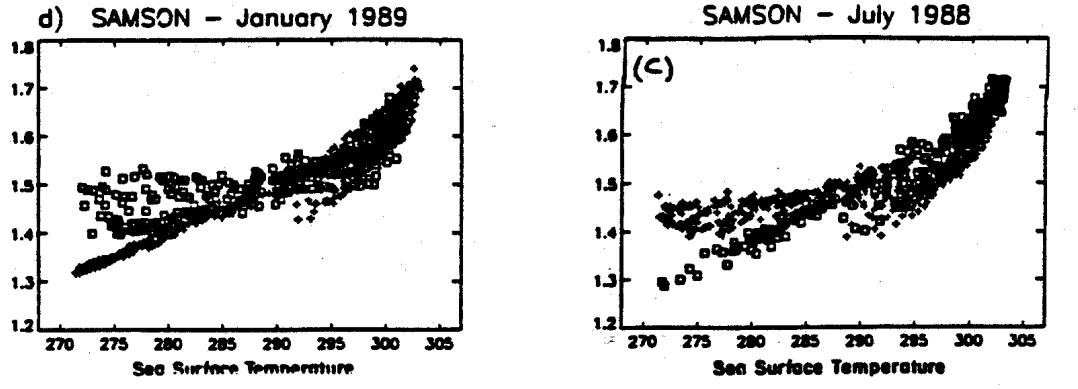

Fig. 6.7 The greenhouse effect as a function of SST with the relationships derived from hemispheric data separated for clarity.

Example 6.4: Another estimate of the gray body optical depth

We can use Eqn. (6.17), together with the data listed on Table 6.1 to arrive at an estimate of τ_s for Earth and Venus. For Venus

$$\left(\frac{750}{244}\right)^4 = \frac{3\tau_s}{4} + 1$$

or $\tau_s = 117$. For Earth,

$$\left(\frac{288}{253}\right)^4 = \frac{3\tau_s}{4} + 1$$

or $\tau_s = 0.9$. The parameter τ_s is therefore a direct measure of the strength of the greenhouse effect.

Physical properties of the three inner planets of the solar system

Planet	Distance from sun (10^6 km)	Solar constant (W m^2)	Albedo	T_e (K)	T_s (K)	τ_F^*
Venus	108	2620	0.71	244	750	117
Earth	150	1367	0.31	253	288	0.9
Mars	228	593	0.17	216	220	~ 0

6.4 Post Satellite View of the ERB

Figure 6.8 shows the globally and monthly averaged components of the ERB derived from measurements made on satellites (these are from a composite of various pre-ERBE satellite measurements). Figure 6.9 shows the net flux separated by winter and summer hemispheres. These diagrams highlight the annual cycle in F_{net}, α, and F_∞. Some notable points:

- Upper panel: planetary albedo - note the maximum during NH winter months. This is associated with illumination of snow covered land surfaces.
- Middle panel: maximum emission NH summer related to heating of land masses.
- Lower panel: net flux maximum in SH summer (perihelion) and minimum during NH summer (aphelion). Sun-Earth distance effects on solar insolation produce an annual cycle ~26 W m^{-2} compared to 22 W m^{-2} observed. (Note offset in observations about ~9 W m^{-2}.)

Zonally averaged profiles of the three components are shown in Fig. 6.10a, b and c. Emitted flux distributions show a bimodal distribution with a minimum about the equator (due to deep, cold convection) and maximum in subtropics (clear sky). Albedo increases poleward due to increasing reflectivity of clouds and other reflecting surfaces as the solar elevation decreases. Note areas shaded show both the surplus of net flux and deficit of net flux in the Polar Regions, implying a transport of energy out of the equatorial regions toward the poles (see §6.6). This is the fundamental drive of the atmosphere and oceanic circulations.

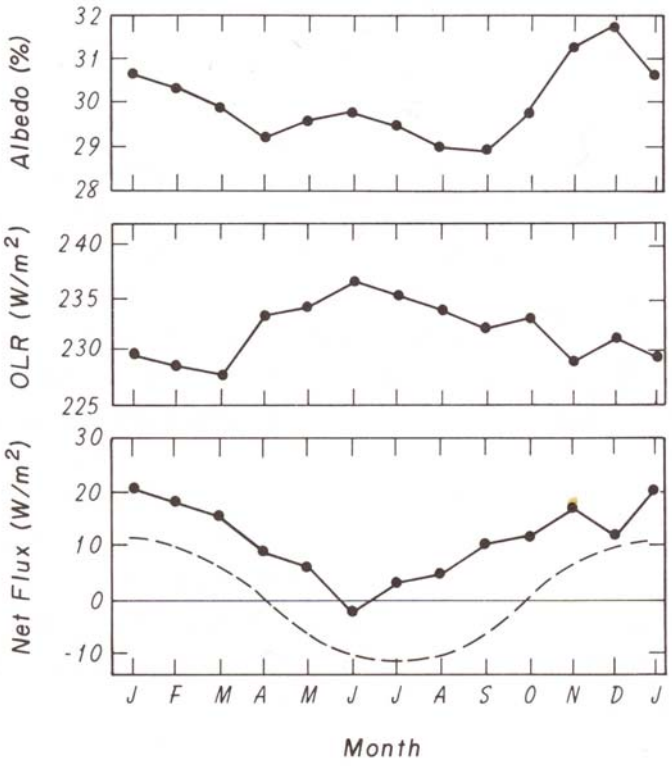

Fig. 6.8 Annual variation of the global albedo, emitted longwave flux and net flux. Also shown in the dashed line is the monthly deviation from the annual mean insolation using a solar constant of 1376 W m^{-2} (after Stephens, et al., 1981).

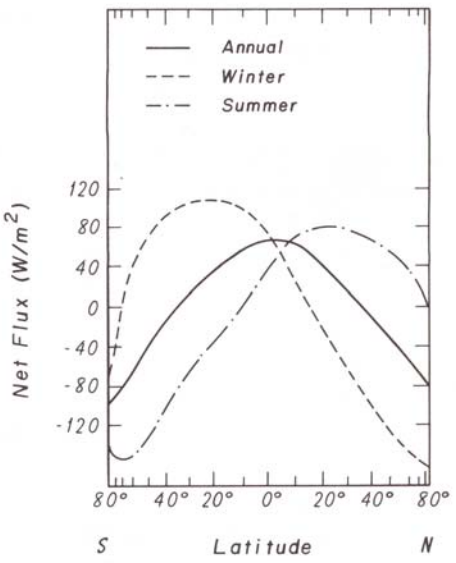

Fig. 6.9 Latitudinal distribution of the annual, winter (December, January, and February), and summer (June, July, and August) net fluxes (after Stephens, et al., 1981, with modifications).

Figs. 6.10a and b show regional distributions of net flux and albedo. These show significant longitudinal variations (e.g., along the equator). The east-west variations in the individual components is as large as the north-south variations. The hot spot of the globe is the maritime continent.

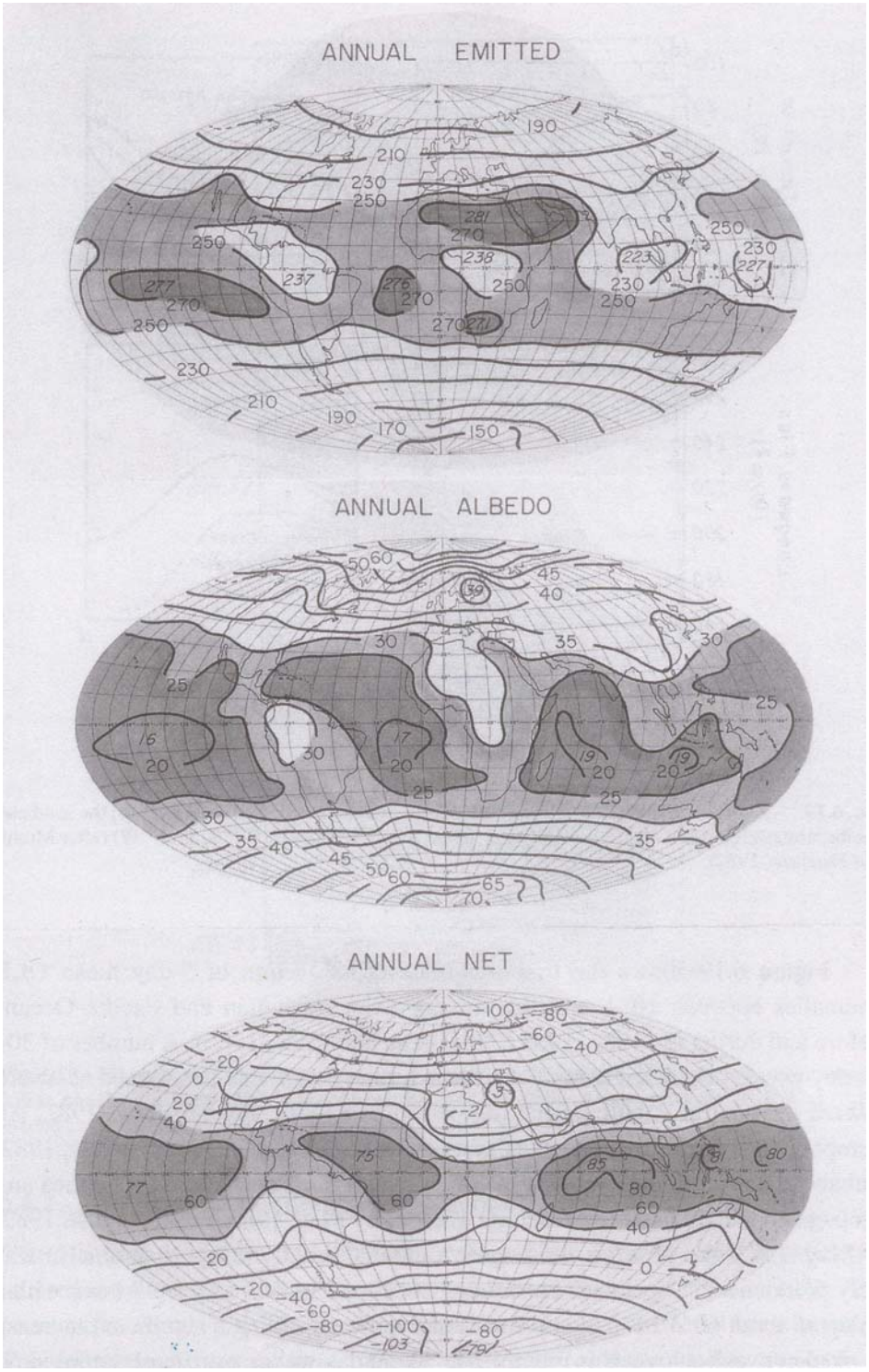

Fig. 6.10 Mean annual infrared flux (W m^{-2}), planetary albedo (%), and net flux (W m^{-2}) (after Stephens, et al., 1981).

6.5 The Energy Budget of Earth

So far we have considered only the part of the budget that applies to the top of the atmosphere. The ERB is also the planetary energy budget since the only exchanges of energy between earth and space take place via radiation. We now examine this energy balance in more detail.

(a) Annual-Global Mean Energy Balance

The annual and globally averaged radiative balance of the atmosphere, unlike for the ERB, is not zero but distinctly negative: *LW* balance = $G - (E + M) - (F + K)$ = -174 W m^{-2} and *SW* balance = $A - D - B$ = 68 W m^{-2}. That is the atmosphere constantly loses energy via radiation by an amount –174 + 68 = -106 W m^{-2} and the earth's surface gains energy by the same amount to balance this loss. Heating of the lower boundary of a fluid while cooling its interior is the classical mechanism for inducing convective instability and turbulence. Turbulent heat transfer (S = 16 W m^{-2}) and condensation of water (the excess of condensation over evaporation—in the form of precipitation falling to the ground, H = 90 W m^{-2}) make up the radiative deficit. The combination of these non-radiative processes is loosely called convective heat transport and the balanced state of the atmosphere is termed at radiative-convective equilibrium.

The surface budget is made up of a balance between net solar radiation at the ground (B = 169 W m^{-2}) plus the net longwave budget at the ground ($E + M – G$ = 63 W m^{-2}) and the heat transferred to the atmosphere via sensible heating (S) and latent heating (H). While the global average shows the transfer of energy ($H + L$) from the surface to the atmosphere, there are times and places where the transfer is in the other direction.

Representations of this budget have varied in detail over the years since the original version of Dines (1917), which is reproduced in Fig. 6.11a. For instance, the planetary albedo, estimated by Dines to be 50%, has been considerably revised to the value of D/A = 30%, largely because of modern satellite ERB measurements. One issue of concern to Dines at the time of his study was the precise value of the Stefan-Boltzmann constant.

(b) Schematic View of IR Radiative Transfer in the Atmosphere

An important observation noted above is that the atmosphere loses IR radiation by the amount of -174 W m^{-2}. This gives rise to an overall atmospheric cooling (to be discussed later). This is a result of longwave radiative transfer in the atmosphere. Longwave radiation is absorbed, emitted and to a much lesser extent scattered from layer to layer in the atmosphere thus creating a transfer problem of some complexity. The chief absorbers of this radiation are:

- Trace gases - CO_2, H_2O and O_3 (these absorptions are quantized processes, which produce discrete absorption "lines". The absorptions occur through quantization of rotation and vibration of the molecular bands and is discussed in more detail in the next chapter).
- Cloud droplets and crystals.
- Aerosol (such as dust, soot, etc.).

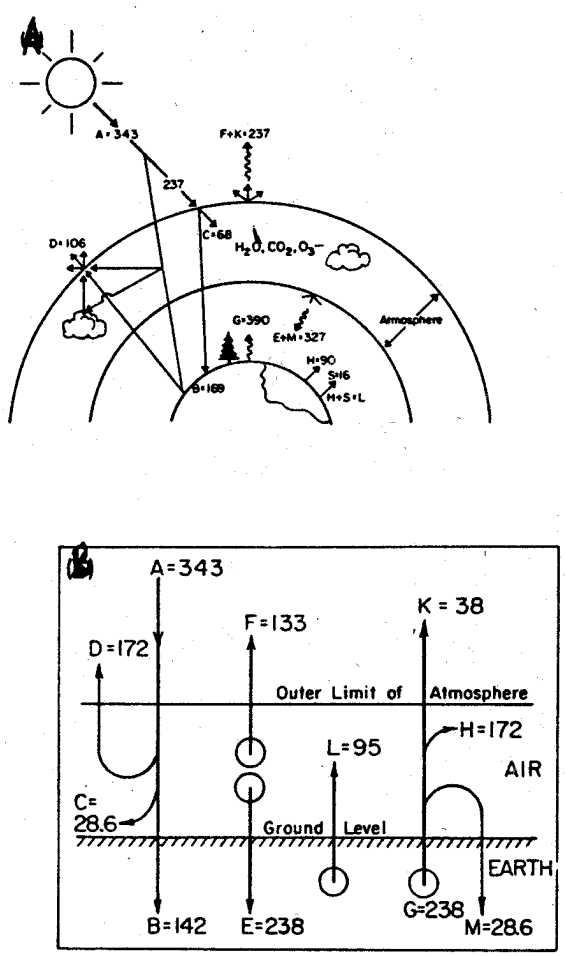

Fig. 6.11 (a) The modern view of the energy budget (Stephens and Tsay, 1991). (b) Original view of the energy budget of the planet as envisaged by Dines (1917).

Figure 6.12a provides a schematic of the longwave flux measured at the ground. This flux is a result of radiative transport processes in the terrestrial atmosphere. Of particular importance to the energy budget of the Earth-atmosphere system is the so called "atmospheric window", which is fairly transparent to radiation processes in the clear atmosphere but this is "filled in" by cloud. Figure 6.12b provides an example (the reverse of Fig. 6.12a) of radiation emitted by Earth and other planets. The radiation is expressed as an equivalent temperature, which is the spectral equivalent of T_p. It is this kind of measurement that enables us to deduce the composition of planetary atmospheres via remote sensing.

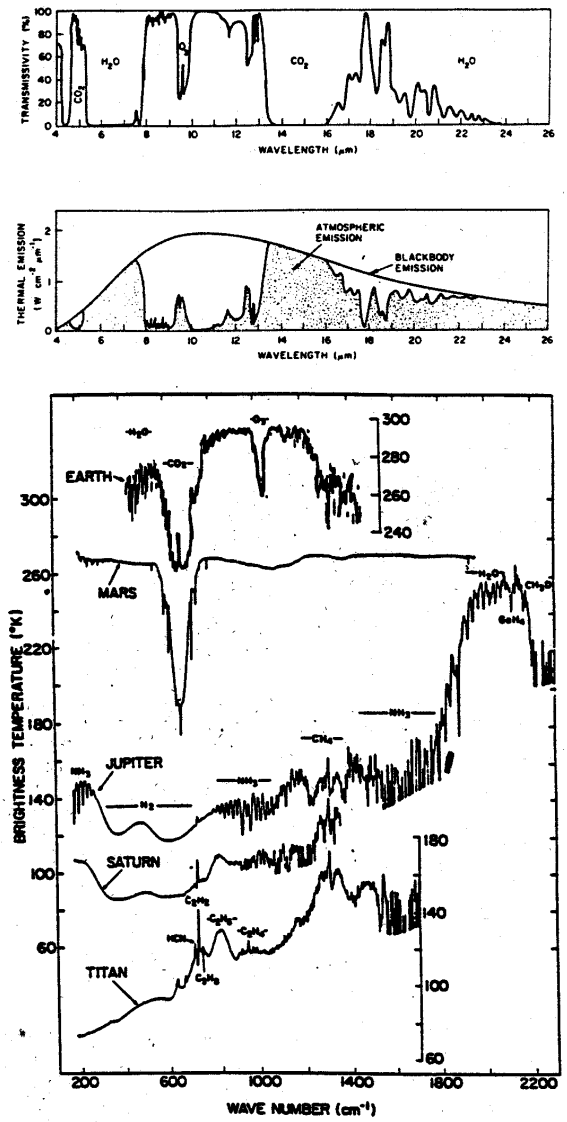

Fig. 6.12 (a) The emission from a clear sky (solid curve) and a cloudy sky (dashed curve) measured by a hypothetical radiometer on the ground. (b) A low-resolution depiction of the absorption by the main greenhouse gases of the Earth's atmosphere (upper part of (b)) spectra of IR emission, plotted as brightness temperatures, for four planets and Titan (Hanel, 1983).

6.6 The Meridional Transport of Heat by the Planet

(a) Observations

The profound role of the general circulation on temperature is illustrated by reference to Fig. 6.13. Without horizontal transport of heat, the temperature of each latitude would be governed by radiative equilibrium alone. In this case, summers in mid-latitudes would be warmer than without transport, and winters much colder. Heat is transported by the atmosphere and oceans out of the equatorial regions and subtropics to the Polar Regions where it is mixed mechanically to produce more moderate temperatures at higher latitudes

(Additional reference, Oort and Vonder Haar, 1976: On the observed annual cycle in the ocean-atmosphere heat balance over the Northern Hemisphere, *J. Phys. Ocean.,* **6**, 781-800.)

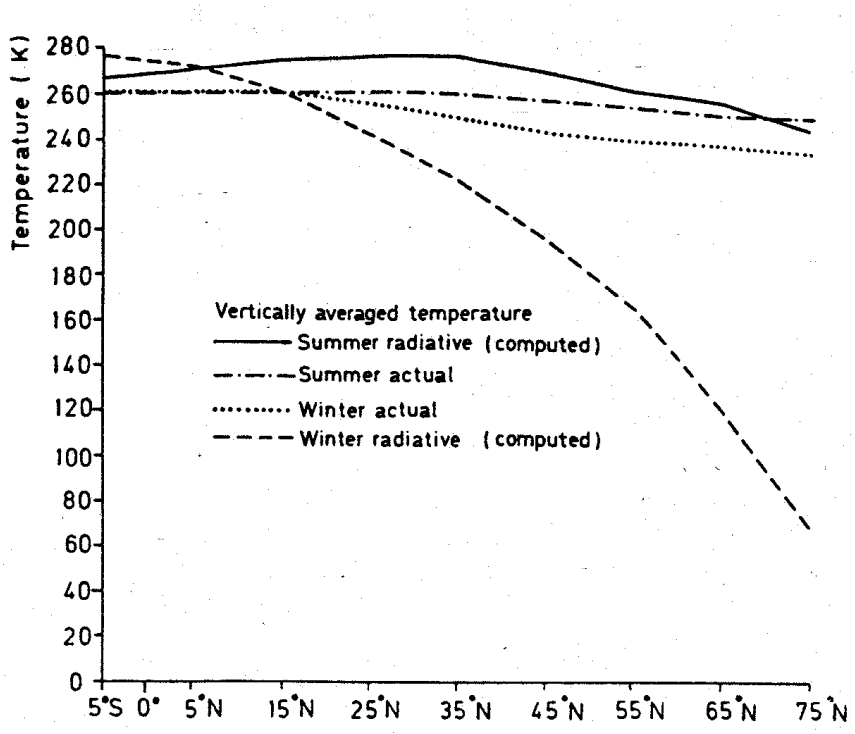

Fig. 6.13 Comparison of theoretically derived radiative equilibrium and observed vertically averaged temperature profiles for the summer and winter.

We can calculate this total transport required from simple principles of energy conservation. Consider the 'system' as in Fig. 6.14 that loses (or gains) energy through its upper boundary and transports energy across its lateral boundaries. The rate at which energy changes inside this system is

$$\frac{\partial E}{\partial t} = F_{net} - div\mathbf{T}_{\mathbf{A}} - div\mathbf{T}_{\mathbf{o}} \tag{6.20}$$

where

- F_{net} = net radiation input into the top of the atmosphere (e.g., Fig. 6.15)
- $div\mathbf{T}_{\mathbf{A}}$ = divergence of energy from the atmosphere due to atmospheric transports
- $div\mathbf{T}_{\mathbf{o}}$ = divergence of energy from the ocean due to oceanic transports.

$\partial E/\partial t$ is the energy gained by the "system" which is then stored in the atmosphere and ocean, i.e.,

$$\frac{\partial E}{\partial t} = S_A + S_o + S_L + S_I \tag{6.21}$$

where S_A, S_o, S_L, and S_I are energy storage terms associated with the atmosphere, ocean, land, and ice, respectively.

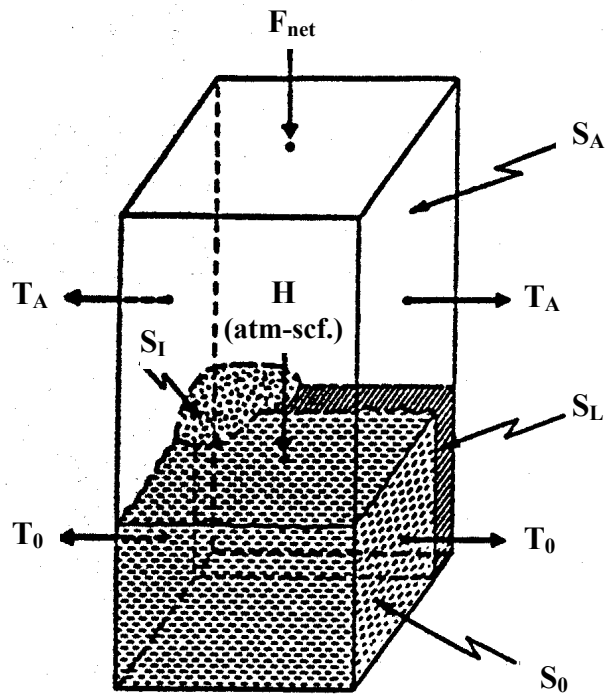

Fig. 6.14 Schematic diagram of the different terms in the earth's energy balance (Oort and Vonder Haar, 1976).

Figures 6.15a and b provide zonally averaged estimates of heat storage by the atmosphere and oceans, respectively (i.e., of S_A and S_o) as a function of time year. The atmosphere storage plays only a minor role in the energy budget. This storage occurs by incoming solar energy, which is used to increase internal energy (temperature), and the specific humidity (i.e., latent energy). The maximum storage occurs around May and maximum depletion is around September. By contrast, the storage of energy by the oceans plays a far more formidable role in the time varying energy budget of the climate system. This reaches a maximum in excess of 100 W m^{-2} at about 40°N. Most of the storage occurs east of North America in the Gulf and east of Japan. The land and ice storage terms are smaller although estimates of S_I are poorly based.

On the annually averaged basis, we consider each latitude zone to be in steady state, i.e.,

$$\left\langle \frac{\partial E}{\partial t} \right\rangle = 0 \tag{6.22}$$

where < > is an annual average.

Thus,

$$\langle F_{net} \rangle = \langle divT_a \rangle + \langle divT_o \rangle \tag{6.23}$$

or

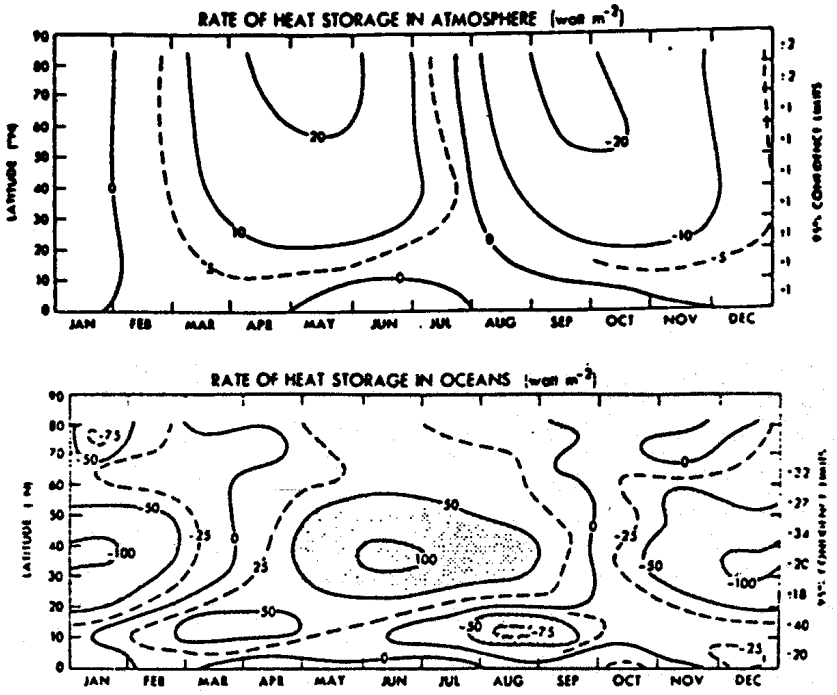

Fig. 6.15 (a) Rate of heat storage in the atmosphere (S_A) based on radiosonde data as a function of latitude and month of the year. Units are in W m^{-2}. (b) Rate of heat storage in the oceans (S_o) based on hydrographic stations, MBT and XBT data as a function of latitude and month of the year. Units are in W m^{-2}. To obtain typical oceanic values divide by the percentage of the horizontal area covered by oceans (factor = 0.61 for the Northern Hemisphere as a whole).

$$\langle F_{net}(\phi)\rangle = \frac{1}{a}\frac{\partial T}{\partial \phi} \tag{6.24}$$

where a is the mean radius of the earth and ϕ is latitude and T is the combined oceanic and atmospheric transport. We can numerically integrate Eqn. (6.24) to obtain the transport required to balance the net radiation deficits (e.g., Carrissimo et al., 1985: Estimating the meridional energy transports in the atmosphere and oceans, *J. Phys. Ocean,* **15**, 82-91). For example, integration of Eqn. (6.24) over the polar cap (Fig. 6.16a) yields

$$T(\phi) = T_a(\phi) + T_o(\phi) = 2\pi a^2 \int_{\pi/2}^{\phi} \langle F_{net}\rangle(\phi')\cos\phi' d\phi' \qquad \text{(W)} \tag{6.25}$$

The total transport is estimated this way using satellite data for F_{net}. The meridional energy transports by the atmosphere may be obtained from analysis of conventional meteorological data (e.g., Oort and Vonder Haar). The ocean transports (Fig. 6.16b) can be derived as a residual.

An alternate way of estimating the heat transport by the Earth's oceans is to consider the average form of the terrestrial branch of the energy balance, i.e.,

$$\langle F_{net-surf}\rangle = \langle div\mathbf{T_o}\rangle \tag{6.26}$$

where, on an annual average basis, the storage terms are zero. The estimate of the oceanic energy transport derived according to this balance is also depicted in Fig. 6.16b (after Sellers). The significant discrepancy between the two estimates has been a topic of debate for some time.

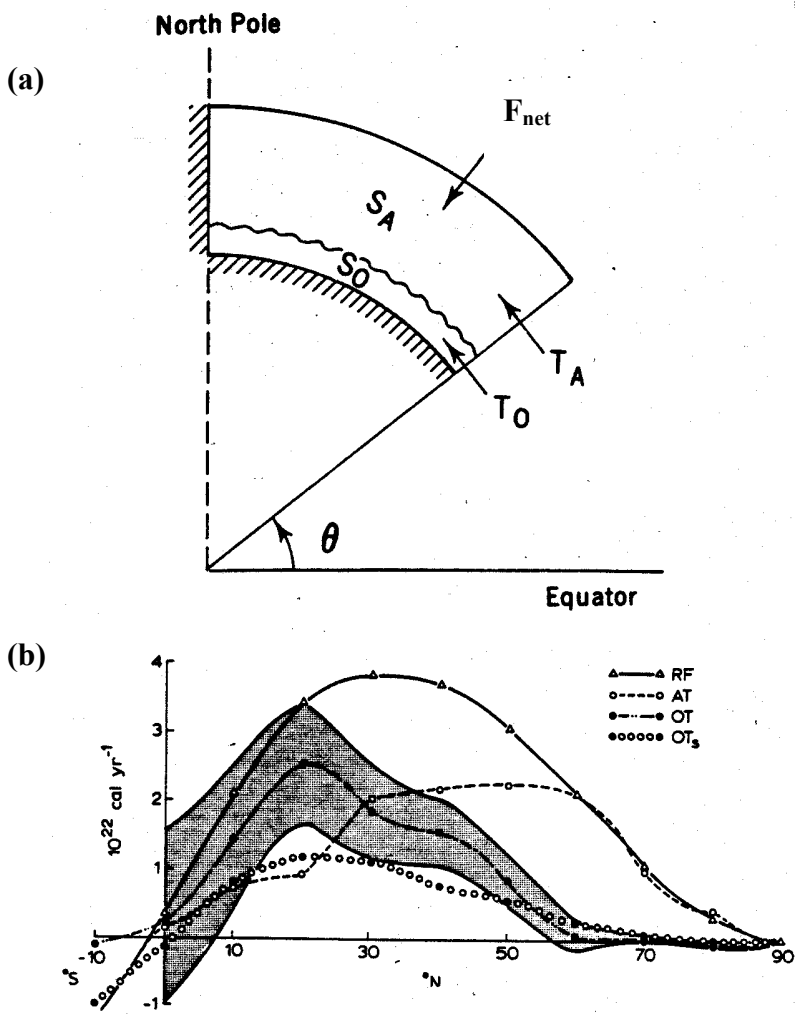

Fig. 6.16 (a) Principle of integration over the polar cap. (b) Variation of net energy transport with latitude over the northern hemisphere: RF = total required energy transport inferred from satellite measurements; AT = measured energy transport by the atmosphere; OT = oceanic energy transport derived from RF and AT; OT_s = oceanic energy transport according to Sellers (1965). Uncertainty in the OT values is denoted by the shading. Minus values indicate net transport to the south (after Vonder Haar and Oort, 1973).

The heat flux distribution around the oceans, based on a similar analysis of the surface budget, is depicted in Fig. 6.17a. The fascinating aspect of the analysis portrayed in this diagram is the consistent northward transport depicted for the entire Atlantic Ocean. However, we should view this analysis as being somewhat speculative given the comparisons of Fig. 6.17a and b. The only real convincing estimate of heat transport of the oceans is from direct estimates from measurements conducted in the ocean. Figure 6.17b shows the results of these kinds of estimates in limited portions of the ocean. The two estimates of Fig. 6.17a and b are broadly similar but differ in important detail.

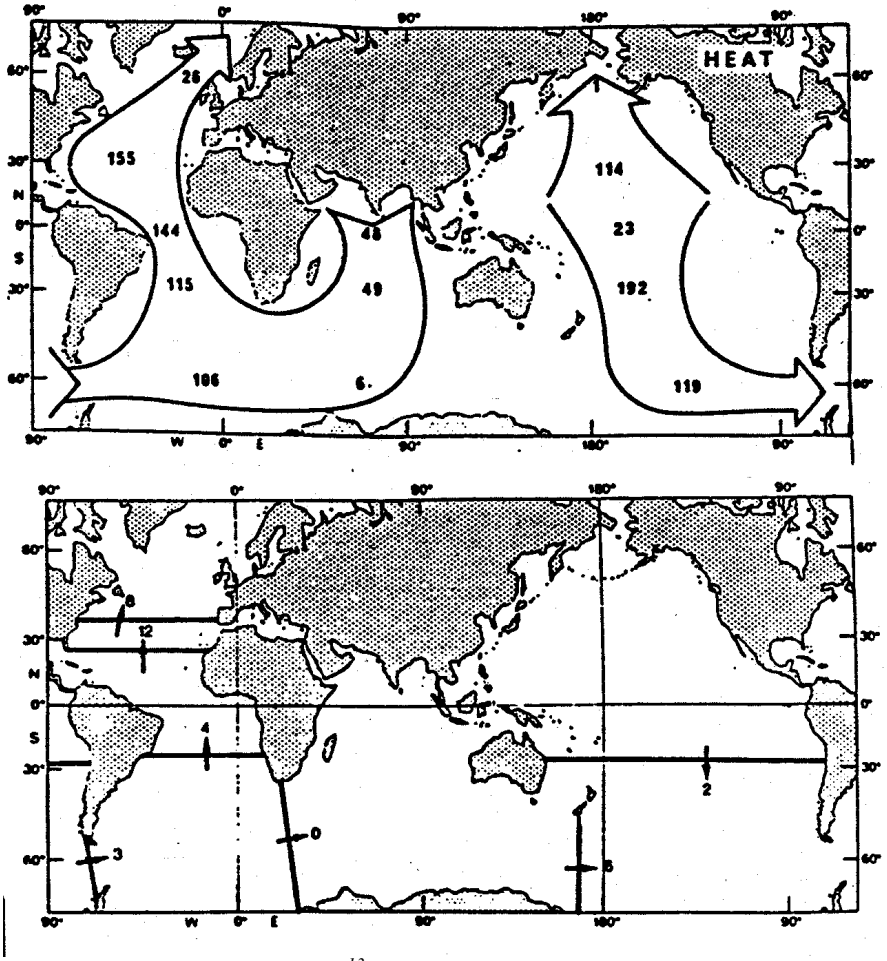

Fig. 6.17 (a) The circulations of heat (10^{13} W) around the world ocean, as deduced by Strommel (1979) and Baumgartner and Reichel (1975) from the global patterns of energy. (b) The circulation of heat 10^{14} W in the world ocean deduced from oceanographic measurements at a few trans-ocean sections (Bryden 1982).

(b) Model Comparisons with Observation

(ref Glecker et al., 1995: Cloud radiative effects on implied energy transports as simulated by AGCMs, *Geophys. Res. Letters*, **7**, 791-794.)

Recent model comparisons have revealed how radiation processes in clouds in different AGCMs lead to an unacceptable large spread in the implied meridional transport. Figure 6.18a shows T_{O+A} inferred from TOA net radiation as observed from ERBE and derived from ERB simulations from models. Figure 6.18b is the atmospheric component of this total transport as deduced from observations (Oort), analyses (Trenberth/Savijarvi) and derived from models. Figure 6.18c shows the zonal average net surface energy flux as simulated from models and as derived from observations (complete with error estimates on the latter). Various observational estimates of T_o are given in Fig. 6.18d and these are contrasted with model deduced transports on Fig. 6.18e also derived from model surface fluxes. The spread in these results and the difference from 'observations' was attributed by Glecker et al. to model differences in treatment of the radiative effects of clouds (Fig. 6.18f). The quantity shown in Fig. 6.18f is the quantity C_{SW} introduced in the next section. When the combined transport of Fig. 6.18a and the atmospheric transports of each model (Fig. 6.18b) are used, the residual ocean transport of Fig. 6.18g is obtained. Together Fig. 6.18f and g

suggest that the implied energy transport in the oceans is not correct largely as a result of poorly represented cloud-radiation processes.

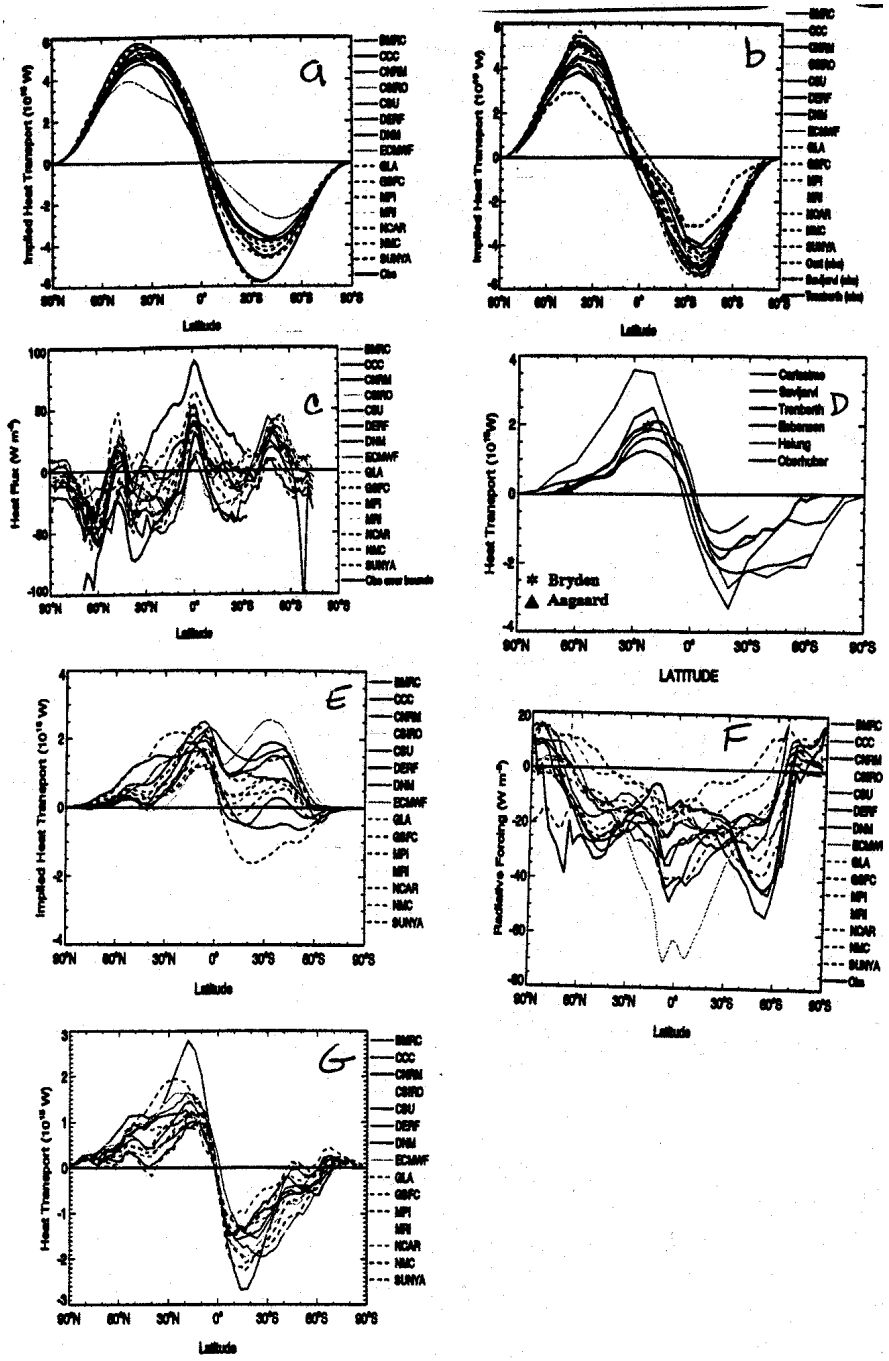

Fig. 6.18 *(a) Annual mean northward meridional energy transport of oceans plus atmosphere. (b) Annual mean northward meridional energy transport of the atmosphere. (c) Net ocean surface heat flux, (d) Observed annual mean northward meridional energy transport of the ocean. (e) Annual mean northward meridional energy transport of the ocean derived from model surface fluxes. (f) Zonal, annual average net TOA cloud flux differences as defined in the next section. (g) Annual mean northward meridional energy transport of the ocean derived from model atmospheric transport and observed TOA ERB.*

6.7 Problems

Problem 6.1

Suppose that a cloud layer whose temperature is 7°C moves over a snow surface whose temperature is 0°C. What is the maximum rate of melting of the snow that could be supported by net LW radiation convergence at the surface if the absorptance of the cloud is 1.0 and of the snow is 0.95?

Problem 6.2

If one assumes that the planetary albedo of the earth is 30%; that the atmosphere transmits all SW radiation; and that the atmosphere acts as a single isothermal layer that absorbs all longwave radiation falling on it, find the radiative equilibrium temperatures of the atmosphere and the earth's surface.

Problem 6.3

A so-called greenhouse is depicted below. Assume a solar zenith angle θ, that the top of the house transmits all SW radiation and has an infrared emittance ε_{TOP}. The ground absorbs all LW radiation and has an albedo ρ_{grnd}. Assuming radiative equilibrium, derive an expression relating the temperature of the ground to the emittance of the roof and the solar zenith angle. Derive a second expression for the equilibrium temperature of the roof as a function of the ground temperature if $\varepsilon_{TOP} = 1$ and $\rho_{grnd} = 0.2$.

Problem 6.4

If the average surface temperature of the earth is 288° and the average albedo of the earth and atmosphere for solar radiation is 30%, find the "effective absorptance" of the atmosphere for longwave radiation.